AIAA JOURNAL
Vol. 31, No. 12, December 1993

Computation of Unsteady Viscous Flow Using a Pressure-Based Algorithm

Y.-H. Ho* and B. Lakshminarayana†
Pennsylvania State University, University Park, Pennsylvania 16802

The objective of this research is the development of an efficient and accurate numerical analysis for the prediction of unsteady turbulent flows using a Navier-Stokes solver. The technique developed is to be used for incompressible flow and is an extension of the pressure-based method. The finite volume approach and a nonstagger grid formulation are used. A predictor-corrector type algorithm is applied to the governing equations to ensure time accuracy. The convergence is improved using a multigrid scheme. A low Reynolds number form two-equation turbulence model is used to simulate the turbulent flow. The code is first calibrated against existing analytical solutions for an oscillating flat plate. To test the two-equation model, a steady-state flow calculation is made and compared with the available experimental data for a turbine stator. Good agreement is obtained between the prediction and the experimental results. The prediction of unsteady viscous flow through a flat plate cascade subjected to a transverse gust is presented. Finally, unsteady flow through a compressor cascade subjected to a gust is predicted and compared with the experimental data. The unsteady blade pressure distribution and the time-dependent wakes are well-captured.

Nomenclature

a_i = coefficients in discretized equations [Eqs. (5) and (6)]
C = chord length
C_{Fw} = aerodynamic force coefficient
C_p = pressure coefficient, $(p - p_1)/Q$
C'_p = pressure coefficient, $(p - p_1)/\rho U_0 v_d$
F = force on the blade surface
G^k = grid index in the multigrid technique
I_k^{k+1} = the restriction operator
k = turbulent kinetic energy, wave decay rate
p = static pressure
p_0 = stagnation pressure
Q = unit control volume/inlet dynamic head
Re = Reynolds number based on mean streamwise velocity/laminar viscosity/the axial chord
s^u, s^v = source terms in u and v equations
U = freestream total velocity
u, v = axial and tangential velocity
u_i = mean velocity tensor
u'_i = fluctuating velocities
v_d = amplitude of the gust velocity
W = wake total velocity
x, y = axial and tangential coordinate
x_i, x_j = Cartesian coordinates
ΔCp = magnitude of unsteady pressure
Δt = time step
δ = boundary-layer thickness
ϵ = turbulence dissipation
ϵ_2, ϵ_4 = coefficients of the artificial dissipation [Eq. (15)]
θ = momentum thickness
μ = molecular viscosity
σ = source term in pressure equation
ρ = fluid mean density
ω = frequency

Subscripts

c = values at the wake center
e = boundary-layer edge
max = maximum value
t = values at the trailing edge
0 = value in the freestream
1 = inlet
2 = trailing edge plane

Superscripts

n = previous time step
$n+1$ = new time step
u, v = coefficients in u and v momentum equations, respectively
$*$ = predictor step
$**$ = first corrector step
$***$ = second corrector step

Introduction

INCOMPRESSIBLE flows comprise a large class of practical engineering problems and are, in many cases, unsteady. Examples include flows around submerged and surface vehicles, low-speed aerodynamic vehicles, and turbomachinery. The computation of incompressible flow involves unique mathematical difficulties that will affect the choice of the numerical method. The primitive-variable formulations are widely used in both two-dimensional and three-dimensional incompressible flows. Most of the present methods that use primitive variables can be classified into one of the following groups: the pseudocompressibility method, the fractional step method, and the pressure-based finite volume method.

In the pressure-based finite volume methods, several different relaxation schemes such as semi-implicit method for pressure-linked equations (SIMPLE, SIMPLEC, etc.) have been applied successfully to incompressible flows. The pressure-implicit with splitting of operators (PISO) technique uses an approach similar to the fractional step methods but employs a predictor-corrector type scheme for the discretized equations. The solution accuracy depends on the operation-splitting number. A two-step corrector scheme for incompressible flow calculation was proposed by Issa[1] to preserve the accuracy. Because of the elliptical nature of the pressure formulation and the requirement that the pressure equation be solved twice in each time step, an efficient matrix solver will become the

Presented as Paper 91-1597 at the AIAA 10th Computational Fluid Dynamics Conference, Honolulu, HI, June 24-26, 1991; received April 4, 1992; revision received April 26, 1993; accepted for publication April 26, 1993.

*Graduate Student, Department of Aerospace Engineering. Student Member AIAA.

†Evan Pugh Professor, Department of Aerospace Engineering. Fellow AIAA.

critical issue in this scheme. Jiang et al.[2] have utilized the pressure-based method to predict vortex shedding downstream of a cylinder.

The pseudocompressibility suffers from the proper choice of pseudocompressibility parameters (which varies from case to case) and the associated stability problem. The fractional step method is computationally ambiguous in the boundary conditions treatment. PISO has the advantages of simplicity and its success with more sophisticated turbulence models. This scheme is therefore implemented for the unsteady incompressible flow calculation. A numerical method based on Hobson and Lakshminarayana[3] and the PISO method for unsteady flow is chosen for this analysis. An alternate direction implicit (ADI) scheme is used to solve all of the discretized governing equations, including the momentum equations for velocities, Poisson-type equation for the pressure, and the two-equation turbulence model to account for turbulent effects. A multigrid scheme is used to improve the convergence of the pressure equation.

A two-dimensional unsteady code has been developed to predict incompressible, unsteady, viscous flow. The code is validated against analytical solutions, including unsteady flow through a cascade of blades. In addition, the code is used to predict unsteady pressure and wake characteristics in a cascade caused by a transverse gust. The main contributions of this paper lie in developing a time-accurate, Navier-Stokes code based on the existing pressure-based algorithm and the multigrid technique, validating the ability of the two-equation turbulence model for unsteady turbulent flow.

Governing Equations and Technique

The Reynolds-averaged Navier-Stokes equations for two-dimensional, unsteady, incompressible flow in a Cartesian tensor form can be written as

$$\frac{\partial u_i}{\partial x_i} = 0 \tag{1}$$

$$\frac{\partial u_i}{\partial t} + \frac{\partial u_i u_j}{\partial x_j} = -\frac{1}{\rho}\left\{\frac{\partial p}{\partial x_j} - \frac{\partial}{\partial x_j}\left[\mu\left(\frac{\partial u_j}{\partial x_i} + \frac{\partial u_i}{\partial x_j}\right) + \rho\overline{u_i' u_j'}\right]\right\} \tag{2}$$

To simulate the turbulent flow, a two-equation, or k-ϵ turbulence model developed by Chien,[4] is employed.

It is clear from the governing equations that pressure is only indirectly coupled with velocities u and v. An equation for pressure can be derived by taking the cross derivatives of the momentum equations and applying the continuity equation to obtain the Poisson equation. A second option is to discretize the momentum equations first and then substitute them into the continuity equation to express the pressure in terms of u and v. The second approach is chosen in this study. Therefore, the compatibility constraint can be satisfied automatically by using a consistent finite-difference method. The compatibility constraint is

$$\iint \sigma \, dx \, dy = \oint \frac{\partial p}{\partial n} \, ds \tag{3}$$

where σ is the source term for pressure equation and n is the outward unit vector normal to the boundary S that encloses the computation domain. Failure to satisfy Eq. (3) will result in nonconvergent solutions.

To accommodate for complex geometries, the generalized body-fitted coordinates are used. The complete transformed equations can be found in Hobson and Lakshminarayana.[3] A no-slip condition is used on the solid surfaces. The exit velocity is computed by applying the governing equation at the exit. The inlet flow velocities are specified.

For the pressure equation, the normal derivative of the pressure is assumed to be zero at the solid surface, which is a reasonable approach for high Reynolds number flows. Furthermore, the Navier-Stokes computation usually requires dense grids near the solid surfaces; therefore the distance between the first grid point and the surface is very small. Two types of pressure boundary conditions are used at the exit plane. The first is the unsteady Bernoulli equation used to extrapolate the pressure at the exit. In this case, the computational domain downstream should be far enough away to neglect the viscous effect. The second involves specifying the static pressure at the exit, an option commonly used in most computational approaches. The pressure is calculated by assuming that the streamwise gradient is zero at the inlet. Because Neumann boundary conditions are used, the pressure at one grid point must be chosen. This control point is taken to be the midchannel point at the exit plane for a cascade.

Discretization and Numerical Algorithm

A control volume approach is used in the numerical solution of equations. The control volume is illustrated in Fig. 1. The strong conservative form of the transport equations are integrated over the control surfaces. Because of the nonregular geometries encountered in most practical applications, the staggered grid becomes inconvenient and less efficient. Therefore, a nonstaggered grid system is implemented, i.e., all of the variables are located at the grid points whereas the coefficients are calculated at the control surfaces around the grid points. To obtain the coefficients at a control surface, simple linear interpolation is used on the transformation plane.

For temporal discretization, a three-point backward differencing scheme is selected. Thus, second-order accuracy in the time domain is preserved. The standard hybrid differencing scheme, or central differencing plus artificial dissipation,[5] is employed to treat the nonlinear convection terms, whereas the diffusive terms are approximated by the central differencing scheme. All cross derivatives are treated explicitly and considered as source terms. At the exit plane, the influence from outside the computation domain is neglected. It is very similar to the characteristic boundary conditions in the hyperbolic system for subsonic flow. The velocity is calculated directly from the governing equations (two outgoing waves) and static pressure is specified at the exit plane by the unsteady Bernoulli equation (one incoming wave).

Since the pressure is coupled with velocity indirectly through the continuity equation, the discretized Poisson equation for pressure has to be solved. The Poisson equation is derived by substituting the discretized form of the momentum equation into the continuity equation. The algorithm suggested by Issa[1] is incorporated in the present unsteady flow calculation. The Cartesian coordinates will be used to demonstrate the concept behind this scheme.

Using the control volume concept, the finite difference equations are obtained by integrating the momentum equations over each control volume and expressing the variations

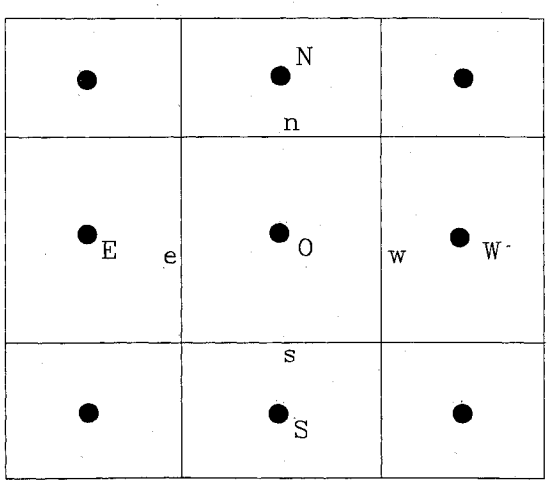

Fig. 1 Control volume for node O and the surrounding control volume.

of u_i in each coordinate direction by suitable schemes (for example, the upwind differencing for the convection term, and central differencing for the diffusion term). The result of this discretization for the u-momentum equation is as follows (Fig. 1):

$$\left(a_o^u + \frac{\rho \Delta Q}{\Delta t}\right) u_o^{n+1} = \sum a_i^u u_i - \frac{\partial p}{\partial x} + S^u + \frac{\rho \Delta Q}{\Delta t} u_o^n \qquad (4)$$

where ΔQ represents the control volume, a_i are the coefficients of the neighboring points after the discretization, a_o is the coefficient for node o, and S^u is the source term.

PISO is a time-marching procedure. During each physical time step there is a predictor step and one or more corrector steps. Issa[1] suggested that the two-step corrector scheme should be sufficient to ensure the divergent-free velocity field and ensure second-order accuracy. During the numerical experiments, this fact was also confirmed.

The discretized equation is first recast into an incremental form which is believed to be more efficient and more accurate in reducing the truncation error. This form also minimizes the computation effort and reduces storage requirements. The converged solution at a previous time step is denoted by a superscript n, whereas the solutions at the present time step are denoted by a superscript * at the predictor level, ** at the first corrector step, and *** at the second corrector step.

For the predictor step, Eq. (4) can be expressed implicitly as

$$\bar{a}_o^u u_o^* = \sum a_i^u u_i^* - \frac{\partial p^n}{\partial x} + S_u^n \qquad (5)$$

and then the first corrector step is

$$\bar{a}_o^u u_o^{**} = \sum a_i^u u_i^* - \frac{\partial p^*}{\partial x} + S_u^n \qquad (6)$$

where $\bar{a}_o^u$ is the coefficient for control volume node O (Fig. 1). Here $\bar{a}_i^u$ are the coefficients of grid points around point O.

Subtracting Eq. (5) from Eq. (6) results in an equation for u_o^{**}

$$u_o^{**} = u_o^* - \frac{1}{\bar{a}_o^u}\left(\frac{\partial p^*}{\partial x} - \frac{\partial p^n}{\partial x}\right) \qquad (7)$$

A similar expression can be derived for v^* and v^{**}. Substitution of Eq. (7) and a similar equation for v^{**} into the continuity equation leads to the pressure equation, which is

$$c_o(p_o^* - p_o^n) = \sum c_i(p_i^* - p_i^n) + B \qquad (8)$$

where $B = u_w^* - u_e^* + v_s^* - v_n^*$, the subscripts e, w, s, and n denote the control surfaces (Fig. 1), and c_o, c_i are the coefficients of pressure for the grid point O and grid points surrounding it. This is the predictor equation for the pressure.

The next set of corrector equations can be derived by expressing Eq. (4) as

$$\bar{a}_o^u u_o^{***} = \sum a_i^u u_i^{**} - \frac{\partial p^{**}}{\partial x} + S_u^n \qquad (9)$$

and subtracting Eq. (6) from the preceding equation leads to a second corrector equation for velocity.

$$u_o^{***} = u_o^{**} + \frac{1}{\bar{a}_o^u}\left[\sum a_i^u (u_i^{**} - u_i^*) + \left(\frac{\partial p^{**}}{\partial x} - \frac{\partial p^*}{\partial x}\right)\right] \qquad (10)$$

A similar equation can be derived for v^{***}. Similar schemes can be devised for the pressure corrector equation.

The turbulent transport equations for the kinetic energy and dissipation rate are strongly coupled with each other and with the momentum equations. However, in order to apply the same algorithm, a similar predictor-corrector operation, which is an implicit predictor step and an explicit-type corrector step, is employed for both equations in each time step.

This numerical scheme can be summarized by the following procedure:

1) The coefficients of the momentum equations are calculated by using the previous time step solutions (u^n, v^n, p^n). This system of equations is solved implicitly. This is the predictor step for velocity.

2) The pressure field is updated from this intermediate velocity field by solving Eq. (8). This is the predictor step for the pressure.

3) Correct (first corrector step for velocity) the velocity field from this new pressure field explicitly.

4) From the corrected velocities, recalculate the coefficients of the pressure equation [Eq. (8)] and solve the implicit system of equations to obtain an exact pressure field.

5) From the new pressure field, re-evaluate the velocity field (second corrector step) explicitly.

6) Solve the k and ϵ equations with a procedure similar to that given in steps 1–5. Apply the similar steps to other scalar equations, if necessary.

7) March to the next time step.

As mentioned in the previous section, incompressible flow equations have no separate equation for the pressure. The pressure has to be obtained from the continuity and momentum equations. Convection across the control surfaces must be known to formulate the continuity equation. Although a nonstaggered grid is more suitable for the generalized coordinates, it suffers from the pressure oscillation when the convection along the control surfaces is calculated from the nodal values. To overcome this problem, the pressure weighting scheme of Rhie and Chow[6] is employed. It is used to link the $2\Delta x$ scheme with the $1\Delta x$ pressure variation. The standard pressure correction scheme is used to set up the coefficients of the pressure equation. To improve the converged rate of the mass flow during each time step, the cross derivative terms of the discretized pressure equations are included and treated explicitly as source terms. The source terms of the discretized pressure equation consist of mass error and the cross derivative terms due to coordinate transformation. During the iteration procedure for solving the discretized pressure equation, the cross derivative terms are updated after each iteration to reflect the pressure changes.

For unsteady flow calculation, the initial condition used is the steady-state solution for the same configuration. To ensure that the mass conservation is satisfied during each time advancement, two approaches can be taken. The first approach is to update the coefficients of the predictor step simultaneously with new velocities until the changes are negligible and then go to the corrector step. In the second approach, coefficients are calculated only once and held constant for each time step. The solutions from both approaches seem to agree with each other. Therefore, in the following computation, the second approach is used to reduce the computational effort.

Alternating Direction Implicit and Multigrid Technique

The system of equations generated by the previous discretization procedure are five-point formulations. The direct matrix solver used to invert this matrix is impractical and very time consuming. Therefore, the alternating direction implicit method is chosen. The additional factorization error is introduced. One needs to use the iterations procedure to remove this error. The factorization error is removed by sweeping the computational domain repeatedly until the rms residuals are less than a specified tolerance and the mass error is removed by solving the pressure equation. Thus, the iteration loop is continued until the factorization error and the mass error are removed.

The second technique used to solve the systems of equations is the multigrid technique. When solving an elliptic equation, traditional iteration algorithms, such as successive over relaxation (SOR), are very effective for the first few iterations but

become ineffective thereafter. The idea of the multigrid method is to take full advantage of the iteration methods for smoothing out the high-frequency error in the first few iterations. Recognizing that a wavelength, which is long relative to a fine grid, is shorter relative to a coarse grid, the long wavelength error on a fine grid becomes a short wavelength error on a coarse grid. Therefore, one can apply the iteration method to the fine grid for a few iterations and transfer the smoothed error to a coarse grid, and apply the same iteration procedure to provide a large reduction in error. A sequence of increasingly coarser grids can be used to effectively reduce the low-frequency errors. Once this is done, the fine grid solution is updated by interpolating the corrections determined from the coarser grid calculation, to reflect the removal of the error.

One simple way to construct a series of grids G^k on the same computational domain is to choose every other point on the fine grid for the next-coarser grid. Several different multigrid algorithms have been applied successfully to solve the Poisson equation. The full approximate storage (FAS) algorithm proposed by Brandt[7] is chosen. The basic idea of this scheme is first to solve the pressure equation with a relaxation method and sweep the field several times. When a slow convergence rate is detected, the residuals are calculated and transferred to the next-coarser grid. This procedure is continued until the coarsest grid is reached. Since the coarsest grid consists of only a small number of grid points, the exact solution is calculated, which requires a very small amount of computational work. The correction can then be interpolated back to the next-finer grid.

Two important operators involved in the multigrid approach are restriction and prolongation. Restriction is used to transfer the correction to the coarse grid, whereas prolongation is used to extrapolate the correction back to the finer grid. The simplest restriction operator is simple injection, i.e.,

$$p_{i,j}^{k} = p_{i,j}^{k+1} \tag{11}$$

where superscripts k and $k+1$ represent the coarse and fine grid, respectively.

The prolongation operator is derived from a bilinear approximation. For grid points on the fine grid, which are coincident with the coarse grid, the injection will again be used. For grid points between adjacent coarse grid nodes, the following equations are applied:

$$\begin{aligned} p_{i,j+1}^{k+1} &= \tfrac{1}{2}(p_{i,j}^{k} + p_{i,j+2}^{k}) \\ p_{i+1,j}^{k+1} &= \tfrac{1}{2}(p_{i,j}^{k} + p_{i+2,j}^{k}) \end{aligned} \tag{12}$$

and the grid points surrounding by coarse grid nodes are extrapolated by

$$p_{i+1,j+1}^{k+1} = \tfrac{1}{4}(p_{i,j}^{k} + p_{i+2,j}^{k} + p_{i,j+2}^{k} + p_{i+2,j+2}^{k}) \tag{13}$$

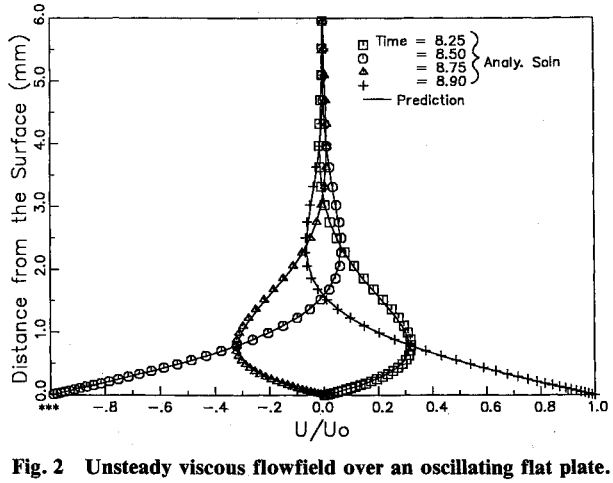

Fig. 2 Unsteady viscous flowfield over an oscillating flat plate.

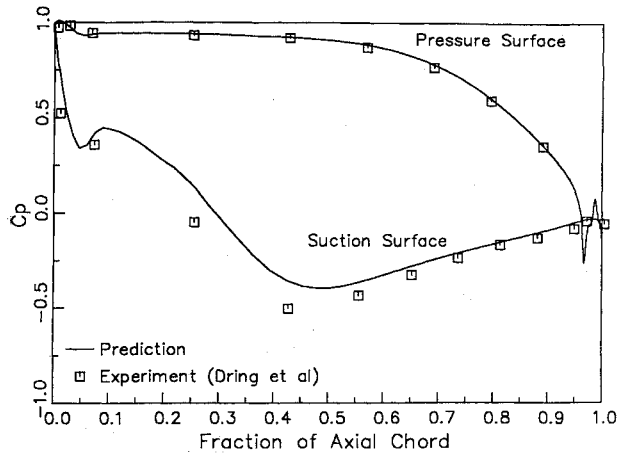

Fig. 3 Prediction and measured blade pressure distribution on a stator blade.

Since the pressure equation in the PISO algorithm is the most critical issue in the unsteady computation, the multigrid technique will only apply to the pressure equation. The coefficients of the pressure equation are calculated on each level of the grid and remain at a constant value during each time step.

Results and Discussion

A pressure-based Navier-Stokes code has been validated against an exact solution for the oscillating flat plate and the experimental data for steady flow through a cascade. The code is then used to predict the unsteady viscous flowfield in a flat plate cascade (subjected to inlet gust) and the unsteady flowfield in a compressor cascade.

Oscillating Flat Plate

The flow over an oscillating plate for which an exact analytical solution[8] is available is computed to validate the algorithm. The mesh is extended in the y direction to 50 points (with stretching to account for the viscous effect near the plate) to assure the far-field boundary condition is satisfied. The problem was run over nine full periods with $\Delta t = 0.01$, after which the solution was fully periodic in time. This test case was also used by Rogers and Kwak.[9] Excellent comparison can be seen from Fig. 2.

Steady-State Flow Prediction

To test the accuracy of the code and the low Reynolds number turbulence model for predicting the turbulent flowfield, the flowfield in the first stator of the Dring et al.[10] turbine facility is computed. The grid consists of 129×61 grid points. The Reynolds number is 0.35×10^6. Since our interest lies in the steady-state solution for this case, the mass conservation constraint need not be satisfied during each time step. The solution requires only three or four sweeps for the pressure field and one sweep for the velocity field to ensure stable solution. Each run takes about 6 h CPU time on a Tektronix XD88/30 workstation. The velocity vector plot at the trailing edge indicates that a recirculation zone exists at the trailing edge and that this flowfield is essentially unsteady. This will cause the steady-state solution to be unstable. A comparison of the computed blade pressure with the experimental data is shown in Fig. 3. The agreement is good except in the high-acceleration region on the suction surface. The wiggle at the trailing edge also confirms the existence of the unsteady recirculation zone. The computed outlet flow angle is 22.2 deg, which also agrees very well with the measured value of 22.4 deg.

The velocity in the wake at 17% of the axial chord downstream is shown compared with the data in Fig. 4. The agreement is excellent for the wake width and the profile except at the wake center. The flowfield in the inviscid region, away from the wake, is also predicted very well.

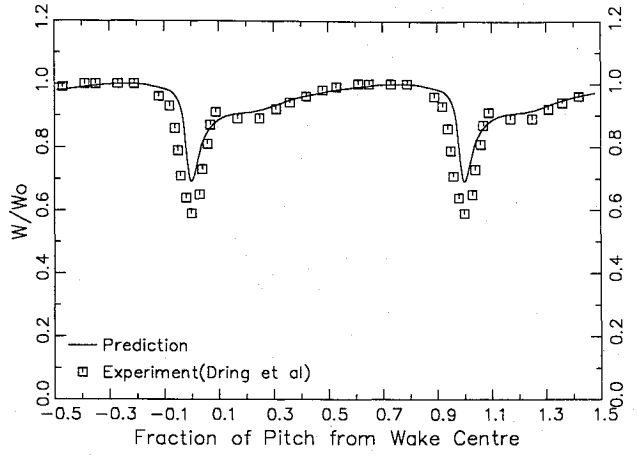

Fig. 4 Predicted and measured wake profile at 17% from the trailing edge of a stator blade.

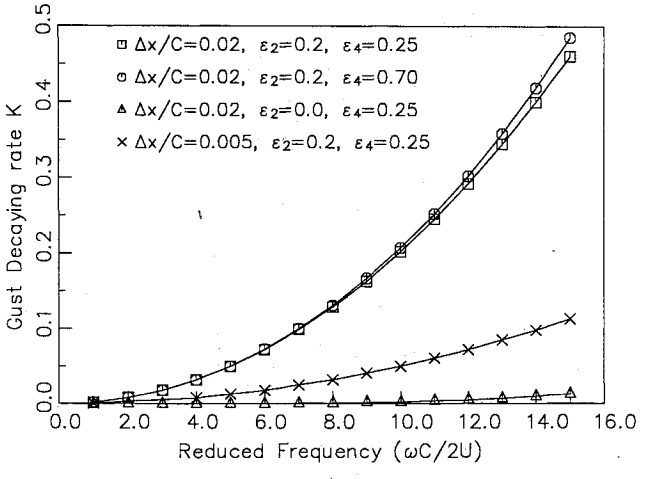

Fig. 5 Effects of the artificial dissipation on the gust decaying rate at different reduced frequencies.

Unsteady Flat Plate Cascade

After achieving confidence in the code through validation, the code was used to compute complex flowfields. One of the cases chosen for this study is the unsteady viscous flow through a flat plate cascade. This is a prelude to the prediction of rotor/stator interaction in turbomachinery. Analytical, inviscid solutions for this case were carried out by Whitehead.[11] The initial inlet freestream velocity is set to 5 m/s, which corresponds to a Reynolds number of 3.4×10^5. The space chord ratio is unity and the stagger angle is 0 deg. Since the flow inside turbomachinery is usually turbulent, turbulence effects become important. To investigate the effects of turbulent flow on the cascade aerodynamic response, the flowfield is computed for a laminar case and turbulent cases (two Reynolds numbers, 3.4×10^5 and 1.0×10^6). The results of these computations should also reveal the influence of the Reynolds number. The computation is carried out at the 5-deg mean incidence. The range of the reduced frequency ($\omega C/2U$) of the transverse gust was chosen to be 0.5–7.5. Nine cases at different flow conditions and reduced frequencies are computed to understand the effects of the frequencies and the Reynolds number. These conditions are shown in Table 1.

The transverse gust is represented by the following expression:

$$U = U_0 i + v_d \sin(\omega t) j \tag{14}$$

where U represents the inlet velocity vector, U_0 the freestream velocity, and v_d the magnitude of the gust. Here v_d is set to 2% of the freestream velocity.

This case represents wake-induced unsteadiness in a turbomachinery stage. The phase angle (between blades) of disturbance felt by the cascade is assumed to be zero. The computational grid consisted of 61×41 points for reduced frequencies of 0.5 and 1.0. For reduced frequencies of 2.5, 5.0, and 7.5, the computational grid was increased to 172×41 points to ensure at least 20 points per wave length at the highest reduced frequencies.

To clarify the dissipative effects of artificial dissipation on the transverse gust, a one-dimensional analysis is performed in free space (without the cascade). The one-dimensional unsteady flow equation in free space is approximated by the finite-difference method. The finite-difference approximation is then substituted in the original equation to prove that the equivalent equation actually solved by the finite-difference method is given by

$$\frac{\partial v}{\partial t} + U\frac{\partial v}{\partial x} = \frac{\epsilon_2}{2}\Delta x \frac{\partial}{\partial x}\left(U\frac{\partial v}{\partial x}\right) - \frac{\epsilon_4}{8}\Delta x^3 \frac{\partial}{\partial x}\left(U\frac{\partial^3 v}{\partial x^3}\right) \tag{15}$$

where ϵ_2 and ϵ_4 are the coefficients of the second- and fourth-order dissipation terms, Δx is the grid spacing, and U is assumed to be constant. This equation was solved to evaluate the effects of ϵ_2, ϵ_4, and Δx on the numerical accuracy at various reduced frequencies.

If a solution of $v(x, t) = e^{-kx}e^{iwt}$ is assumed, the equation for k is

$$\epsilon_4 \Delta x^3 k^4 - 4\epsilon_2 \Delta x k^2 - 8k + 8iw = 0 \tag{16}$$

The results for several combinations of Δx, ϵ_2, and ϵ_4 are shown in Fig. 5. Since there is no physical dissipation, the ideal case will be a traveling gust without any decay, $k = 0$. As shown in Fig. 5, ϵ_2 has a major influence on the decaying rate of the gust and its value should be minimal. The reduced grid spacing has similar effects in reducing the numerical dissipation. Therefore, the first-order upwind scheme is inherently very dissipative (large second-order dissipation) and is not suitable for reduced frequencies higher than one. However, errors introduced into the phase speed are insignificant for all combinations considered here.[12]

For one-dimensional analytical solutions [Eq. (16)], a traveling wave can be resolved accurately with 10 grid points per wavelength (the wavelength for a reduced frequency of 15 is $0.2C$). However, due to the discretization and truncation error, it is found from numerical experiments that at least 20 grids points are required to represent a wave. A combination of the optimum grid size and artificial dissipation coefficients (ϵ_2, ϵ_4) for the convection terms is crucial for the accurate prediction of unsteady flow. The coefficients of the artificial dissipation are limited to the minimum values to maintain a stable solution.

The optimum values of ϵ_2 and ϵ_4, derived from stability consideration, were used in combination with optimum values of Δx (determined through numerical experiments) at each of the reduced frequencies. The standard hybrid scheme is used for reduced frequencies of 0.5 and 1.0. At a reduced frequency

Table 1 Various flow conditions for the flat plate cascade computations

Reduced frequency	Chord length, m	Reynolds number	Laminar turbulent
0.5	1.0	3.4×10^5	Laminar
0.5	1.0	3.4×10^5	Turbulent
0.5	3.0	1.0×10^6	Turbulent
1.0	1.0	3.4×10^5	Laminar
1.0	1.0	3.4×10^5	Turbulent
1.0	3.0	1.0×10^6	Turbulent
2.5	3.0	1.0×10^6	Turbulent
5.0	3.0	1.0×10^6	Turbulent
7.5	3.0	1.0×10^6	Turbulent

of 2.5, the ϵ_2 is set to 0.1 and ϵ_4 is set to 0.3. For reduced frequencies of 5.0 and 7.5, ϵ_2 is set to zero and ϵ_4 is equal to 0.5.

The computed steady lift coefficient for a 5-deg mean incidence is 0.165, whereas the value from analytical solution by Weinig[13] is 0.160. The agreement is good. A typical convergence history for the flat plate cascade is shown in Fig. 6. For the unsteady flow calculation, the initial condition used is the steady-state solution for the same configuration. The steady-state solution is achieved by first advancing 250 time steps. The transverse gust is then turned on to simulate the unsteady flow. In the convergence history shown in Fig. 6 for $\omega C/2U = 1.0$, 250 time steps represent one cycle. The unsteady solution usually does not converge in the first cycle. In the final converged state, periodicity is well-captured. The residuals shown in Fig. 6 are the values before the iteration procedure. It usually requires 10–20 sweeps on the computational domain to reduce the rms residue to less than 10^{-6}. This case requires 2200 s for 1250 time steps on a Cray 2 machine.

To demonstrate the efficiency of the multigrid technique, the flow through a flat plate cascade is computed with three different matrix solvers. These are the line relaxation technique, the ADI technique, and the multigrid technique. The line relaxation technique is chosen as the relaxation solver in the multigrid technique. Therefore, a comparison between the line relaxation technique and the multigrid technique is a precise index of computational effort for single grid and multigrid calculations. The computations are performed on the Pennsylvania State IBM 3090/600S machine. The same numbers of iterations and convergence criteria are set for all of the comparisons. It is found that the four-level multigrid

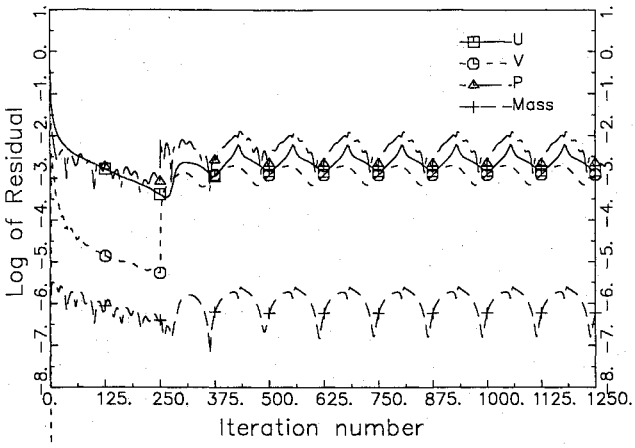

Fig. 6 Convergence history for a flat plate cascade, reduced frequency of 1.0, Reynolds number of 3.4×10^5, laminar flow.

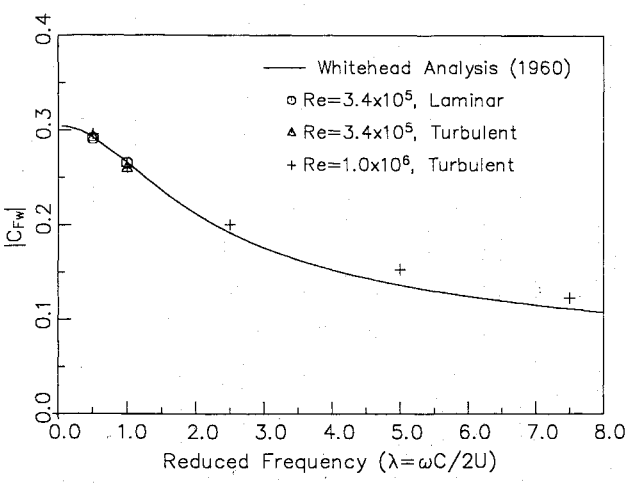

Fig. 7 Effects of turbulent flowfield and Reynolds number on the aerodynamic force function (C_{Fw}) of a flat plate cascade.

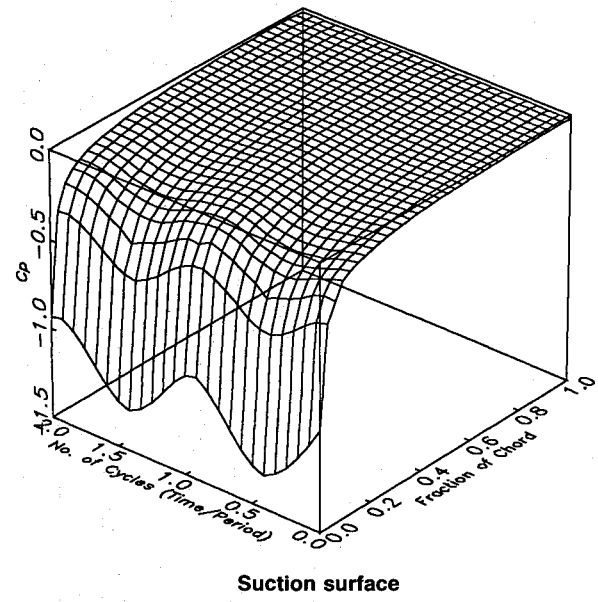

Fig. 8 Pressure time history for reduced frequency 1.0 and Reynolds number 3.4×10^5, turbulent flow.

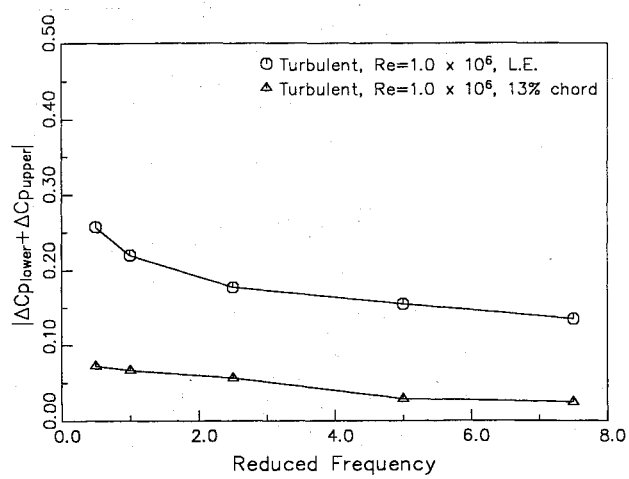

Fig. 9 Frequency dependency of unsteady pressure amplitude at leading edge and 13% of the chord length.

computation is 2.7 times faster than the single grid (line relaxation) and 1.5 times faster than the ADI technique. However, the memory storage requirement for the multigrid technique is 1.3 times larger than it is for the traditional techniques. Since the unsteady flow computation is always performed on high-speed and large-memory computers, it is believed that computational efficiency is more important. Thus, the ability of the multigrid technique to substantially reduce the computational effort has been established.

The blade's unsteady response results are presented in Fig. 7 and compared with the analytical solution.[10] The definition of aerodynamic force coefficients are as follows:

$$C_{Fw} = \text{force coeffs} = \frac{F}{\pi \rho U C v_d} \tag{17}$$

where F is the unsteady force acting on the blade surface.

The agreement is good for all reduced frequencies. It should be remarked here that the flat plate case was chosen to validate the code, even though it is not a good indicator of the actual flowfield in turbomachine blade geometries. Furthermore, the computations carried out are for a low, steady load, where the linearized theories are accurate. It is unlikely that such good agreement will exist between the analytical (inviscid, linear)

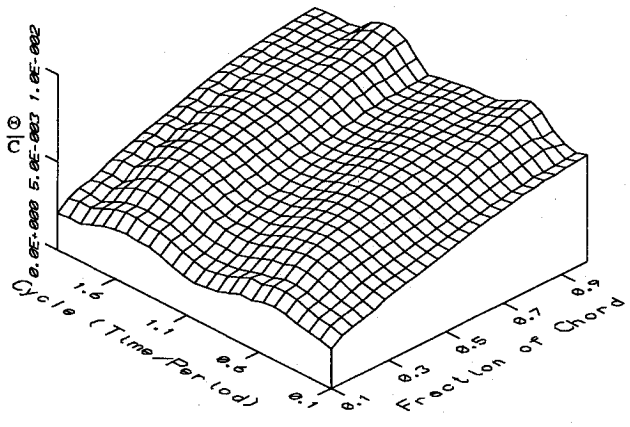

Fig. 10 Momentum thickness time history on the blade suction surface for reduced frequency of 1.0, Reynolds number of 3.4×10^5, turbulent flow.

and Navier-Stokes computations for the heavily loaded, viscous, unsteady flows encountered in practical turbomachine applications.

The instantaneous blade pressure histogram of unsteady pressure is shown in Fig. 8. Only typical results are shown and interpreted here. Comprehensive results are given in Ho.[12] The unsteady pressure envelope is confined to only 25% of the chord length from the leading edge. The response of the blade suction and pressure surfaces to unsteadiness is also quite different. As expected, the unsteady pressures on the blade surfaces are out of phase by 180 deg. The maximum unsteady pressure of the various reduced frequencies at the leading edge and at 13% of the chord length from the leading edge is presented in Fig. 9. At low reduced frequencies, the amplitude of the unsteady blade pressure is high and decreases as the frequency is increased. The unsteady pressures decrease dramatically downstream of the leading edge. For example, at low reduced frequencies, the amplitude decreases by almost 75% from $x/C = 0.0$ to $x/C = 0.13$.

To study the effect of unsteady flow on the momentum thickness, a typical time history of the momentum thickness on the blade suction surface is shown in Fig. 10. The expression for momentum thickness is

$$\frac{\theta}{C} = \int_0^{\delta} \left(1 - \frac{u}{u_e}\right) \frac{u}{u_e} \, \mathrm{d}\left(\frac{y}{C}\right) \tag{18}$$

where u_e is the boundary-layer edge velocity and δ is the edge of the boundary layer.

The temporal variation of the momentum thickness on the pressure surface is negligible. One important feature found (Fig. 10) is that the temporal variation of the momentum thickness is still significant at the trailing edge. However, the unsteady effect on the pressure disappears within 25% of the chord length as was discussed previously (Fig. 8). The flowfield retains history effects. For example, the unsteady pressure near the leading edge causes the growth of unsteady boundary layer. This time dependency (memory) is maintained by the flowfield long after the unsteady pressure field has decayed.

The flow conditions at midchannel at different locations, i.e., inlet, leading edge, trailing edge, and outlet, are shown in Fig. 11 for a reduced frequency of 1.0. The locations are denoted as a–d in Fig. 11. The axial velocity distribution (at a fixed time step) demonstrates that the transverse gust has little effect on the axial velocity. Mass flow conservation is preserved through the flowfield. The differences between the axial velocities at various locations is of the same order of magnitude as the numerical error. The tangential velocity at various locations is also shown in Fig. 11. The wave is convected downstream by the local mean velocity. As the gust approaches the channel, the flow is straightened out (to satisfy the wall boundary conditions) and this has a tendency to decrease the gust velocity. It remains nearly constant downstream of the trailing edge, but there are changes in the phase angle due to the convective velocity.

The temporal behavior of the pressure is quite different from that of the velocity. Since the pressure wave propagates at the speed of sound, the phase angle changes are small. The outlet pressure is nearly steady, indicating that a reasonable

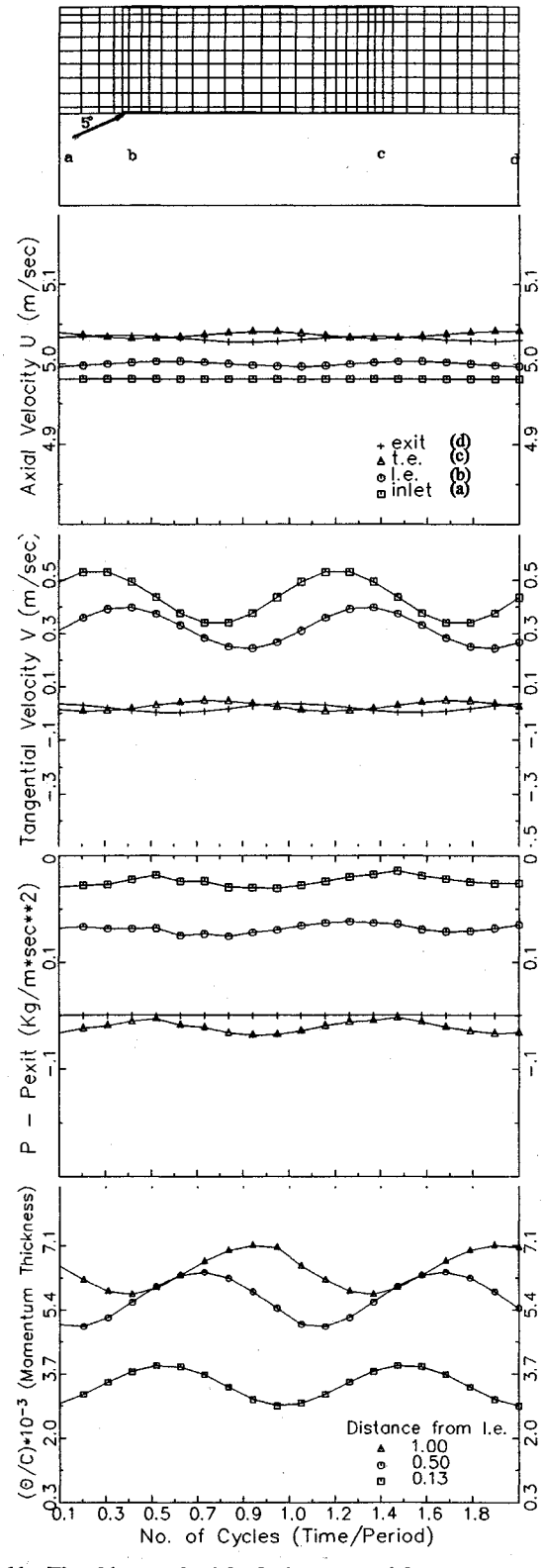

Fig. 11 Time history of axial velocity, tangential velocity, static pressure, and momentum thickness for a flat plate cascade (reduced frequency of 1.0, Reynolds number of 3.4×10^5, turbulent flow).

approach would be to prescribe steady-state conditions at the exit. This is an important result considering the fact that the exit boundary condition in unsteady flow has been a controversial matter in the field of unsteady aerodynamics. However, a word of caution is in order regarding the acoustic computations. A steady-state exit boundary condition for pressure may not be accurate due to the fact that the change in the acoustic pressure is still significant at the exit plane. The variation of the momentum thickness (Fig. 11) on the blade suction surface demonstrates the importance of the initial rate of boundary-layer growth. The initial momentum thickness is about 50% of the momentum thickness near the trailing edge.

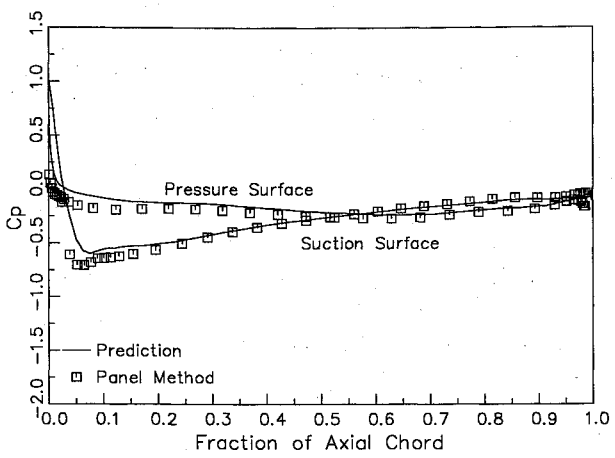

Fig. 12 Steady pressure distribution for the C4 cascade.

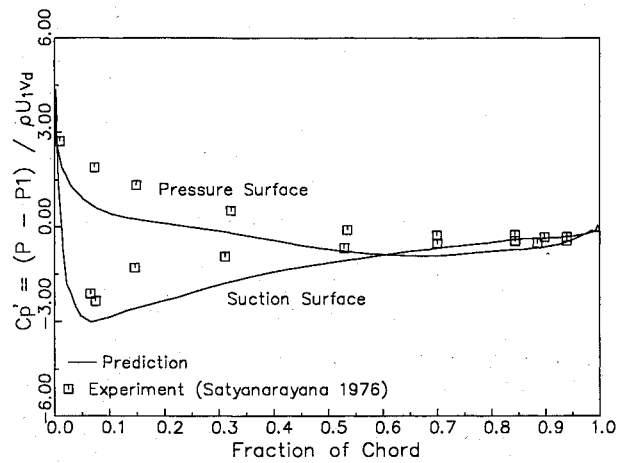

Fig. 13 Maximum unsteady pressure distribution on the C4 cascade.

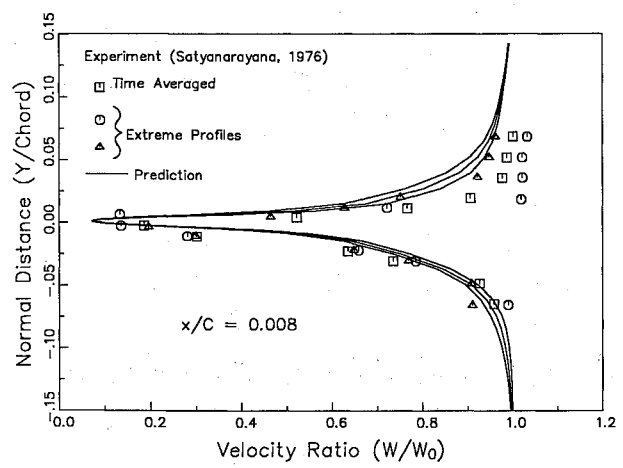

Fig. 14 Unsteady wake at 0.8% chord downstream of the C4 cascade.

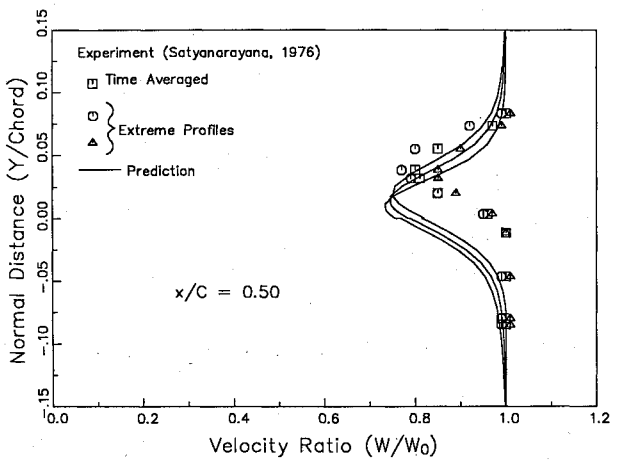

Fig. 15 Unsteady wake at 50% chord downstream of the C4 cascade.

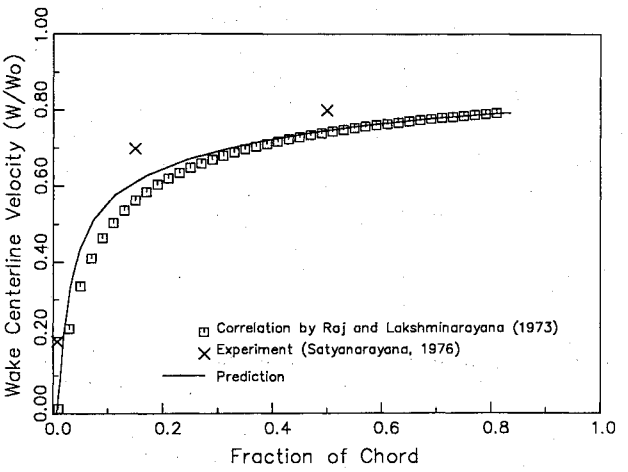

Fig. 16 Variation of the time mean wake centerline velocity downstream of C4 cascade.

The amplitude is almost 25% of the time-averaged value for this low reduced frequency ($\omega C/2U = 1.0$).

Unsteady Flow Through a Compressor Cascade

After a thorough investigation of the unsteady flow through a flat plate cascade, the flowfield in compressor cascade blades of various thicknesses and cambers has been investigated. The cascade chosen for this study is the Cambridge University cascade investigated by Satyanarayana.[14] The transverse gust is generated by moving the wavy walls of the wind tunnel. When the upper and lower walls are in phase, a transverse gust is generated. The cascade, with 10C4 airfoil, stagger angle of 45 deg, and a space/chord ratio of 0.707, has been tested at a Reynolds number of 1.6×10^5. Although there are no turbulence quantities reported, it is believed that turbulence effects are important at this Reynolds number. Therefore, a 1% turbulent intensity is assumed for the inlet condition. The transverse gust is represented by Eq. (14). The magnitude of the gust v_d is 8.2% of the freestream velocity and the reduced frequency is 0.042.

Since there is no steady-state data presented in Satyanarayana's report, the steady blade static pressure computed by the code is compared with the panel code results in Fig. 12. The agreement is good. The maximum unsteady blade pressures are shown compared with the data of Satyanarayana[14] in Fig. 13. The agreement is qualitative even though the maximum change in the local lift is well-predicted. Whereas the computation enforces periodicity, it is not certain whether periodicity existed in the experimental setup. The unsteady

wake profiles at two chordwise distances downstream of the trailing edge of $x/C = 0.008$ and 0.50, respectively, are shown and compared with the data in Figs. 14 and 15. The mean and the extreme (maximum and minimum) wake profiles and the wake center width are well-predicted. The path of the decaying wake is also predicted very accurately. The wake center is only shifted by about 5% of the chord length off the measured value at $x/C = 0.50$. The time-mean wake centerline velocity is plotted against the correlation by Raj and Lakshminarayana[15] shown in Fig. 16. Even though the correlation developed is for a space ratio of 0.664 (the computed space ratio is 0.707), the agreement is very good. The ability of the code to capture the unsteady wake is encouraging.

Concluding Remarks

A two-dimensional unsteady turbulent flow computation technique based on an extension of the pressure correction method has been developed and validated against analytical and/or experimental results. A two-equation turbulence model is integrated with the code to account for turbulence effects.

The major conclusions are as follows for unsteady flow through a flat plate cascade:

1) The Navier-Stokes code is able to accurately predict the aerodynamic forcing function due to an upstream wake and is in good agreement with the analytical predictions for all reduced frequencies.

2) The unsteady Bernoulli equation is a good boundary condition to use at the exit. The computations indicate that the pressures are steady at the exit. This may simplify the prescription of exit boundary conditions in the computation of unsteady flows in turbomachines.

3) The unsteady blade pressure envelope is confined to 20–25% of the chord from the leading edge. The temporal variation of the maximum unsteady pressure can be as high as 20% of its time-mean value at the leading edge at a low, reduced frequency.

4) The temporal variation of the velocity remains significant at the trailing edge. The unsteady velocity field decays slower than the pressure field. This is confirmed by the time-dependent momentum thickness evaluated at the trailing edge.

5) Compared to the traditional matrix solvers, the implementation of the multigrid technique reduces the computing efforts by nearly a factor of three.

The major conclusions are as follows for unsteady flow through a compressor cascade:

1) The ability to compute the unsteady viscous flow through a practical cascade is established by comparing the numerical prediction to the experimental data from a cascade subjected to a transverse gust.

2) Although the prediction of the maximum time-dependent pressure distribution on the blade surfaces does not match very well, the local lift (pressure difference) on the blade is well-captured. The agreement between the computed and measured minimum pressure is good.

3) The agreement between the predicted and the experimental data for two unsteady wakes at two downstream locations are excellent.

Acknowledgments

This work is supported by the Office of Naval Research through Contract N00014-90-J1182 with J. Fein as Contract Monitor. The authors would like to thank A. H. Basson for the grid generation package and comments on the paper. P. J. Morris provided the one-dimensional analysis of the gust decay. Substantial improvement in predictions were achieved through critical and constructive comments by D. E. Thompson and P. J. Morris. The authors also wish to acknowledge NASA for providing the supercomputing resources at the National Aerodynamic Simulation Facility at the NASA Ames Research Center.

References

[1]Issa, R. I., "Solution of the Implicitly Discretized Fluid Flow Equations by Operator-Splitting," *Journal of Computational Physics,* Vol. 62, No. 1, 1986, pp. 40–65.

[2]Jiang, Y., Chen, C. P., and Tucker, P. K., "Multigrid Solution of Unsteady Navier-Stokes Equation Using a Pressure Based Method," AIAA Paper 90-1522, June 1990.

[3]Hobson, G. V., and Lakshminarayana, B., "Prediction of Cascade Performance Using an Incompressible Navier-Stokes Technique," *Journal of Turbomachinery,* Vol. 113, No. 4, 1991, pp. 561–572.

[4]Chien, K.-Y., "Prediction of Channel and Boundary-Layer Flows With a Low-Reynolds-Number Turbulent Model," *AIAA Journal,* Vol. 20, No. 1, 1982, pp. 33–38.

[5]Basson, A. H., "Numerical Simulation of Steady Three-Dimensional Flows in Axial Turbomachinery Bladerows," Ph.D. Thesis, Dept. of Aerospace Engineering, Pennsylvania State Univ., May 1993.

[6]Rhie, C. M., and Chow, W. L., "Numerical Study of the Turbulent Flow Past an Airfoil with Trailing Edge Separation," *AIAA Journal,* Vol. 21, No. 11, 1983, pp. 1525–1532.

[7]Brandt, A., "Multi-Level Adaptive Solutions to Boundary-Value Problem," *Mathematics of Computation,* Vol. 31, No. 138, 1977, pp. 333–390.

[8]White, F., *Viscous Fluid Flow,* McGraw-Hill, New York, 1990, pp. 138–141.

[9]Rogers, S. E., and Kwak, D., "Steady and Unsteady Solution of the Incompressible Navier-Stokes Equations," *AIAA Journal,* Vol. 29, No. 4, 1991, pp. 603–620.

[10]Dring, R. P., Blair, M. F., Joslyn, H. D., Power, G. D., and Verdon, J. M., "The Effects of Inlet Turbulence and Rotor/Stator Interactions on the Aerodynamics and Heat Transfer of a Large-Scale Rotating Turbine Model," NASA CR 4079, July 1987.

[11]Whitehead, D. S., "Force and Moment Coefficients for Vibrating Airfoil in Cascade," British Aeronautical Council Repts. and Memo 3254, 1960.

[12]Ho, Y.-H., "Computation of Unsteady Incompressible Flows in Turbomachinery Applications with the k-ϵ and Instability Wave Turbulence Model," Ph.D. Thesis, Dept. of Aerospace Engineering, Pennsylvania State Univ. (in preparation).

[13]Weinig, F. S., "Theory of Two Dimensional Flow Through Cascades," *Aerodynamics of Turbines and Compressors,* edited by W. R. Hawthorne, Princeton Univ. Press, Princeton, NJ, 1964, Chap. 1.

[14]Satyanarayana, B., "Unsteady Wake Measurement of Airfoils and Cascades," *AIAA Journal,* Vol. 15, No. 5, 1976, pp. 613–618.

[15]Raj, R., and Lakshminarayana, B., "Characteristic of the Wake Behind a Cascade of Airfoils," *Journal of Fluid Mechanics,* Vol. 61, No. 4, 1973, pp. 707–730.